NRIAG JOURNAL OF ASTRONOMY AND GEOPHYSICS
2020, VOL. 9, NO. 1, 71–84
https://doi.org/10.1080/20909977.2020.1711695

Radioactivity and gamma ray spectrometry of basement rocks in Okene area, southwestern Nigeria

M. A. Adabanija[a], O.N. Anie[b] and M. A. Oladunjoye[c]

[a]Department of Earth Sciences, Ladoke Akintola University of Technology, Ogbomoso, Nigeria; [b]Department of Pure and Applied Physics, Ladoke Akintola University of Technology, Ogbomoso, Nigeria; [c]Department of Geology, University of Ibadan, Ibadan Nigeria

ABSTRACT

Abundant outcrops of crystalline rocks in the Okene area, southwestern Nigeria, suggest exposure of the inhabitants to gamma radiation. The power generation of the nation also remains a far cry from the required 20,000 MW, thus necessitating the need for alternative power supply. Therefore, the background radiation level and radiogenic heat potential of crystalline basement rocks in Okene were investigated using gamma ray spectrometry. This was accomplished by analysing 19 rock samples of different lithologies, namely banded gneiss, granite, charnockite, biotite granite, pegmatite and schist, collected from different locations of the Okene area for analysis which involved determining the concentration of U-238, Th-232 and K-40 radionuclides using a Canberra S100 multi-channel analyser with NaI(Tl) detector.

The mean gamma radiation emitted on a lithological basis was in the order pegmatite > charnockite > granite > schist > banded gneiss > biotite granite and yielded an overall mean dose of 63.35 nGy/h corresponding to 3.11 $mSvy^{-1}$ annual effective dose equivalent. The computed radiogenic heat potential indicated banded gneiss has the highest potential, ranging between 0.964 and 1.407 μWm^{-3} with a median of 0.964 μWm^{-3}. Biotite granite has the lowest potential, varying from 0.774 to 1.014 μWm^{-3} with a median heat-generation capacity of 0.894 μWm^{-3}.

The radiogenic heat production varied with lithology, whilst the background radiation annual dose equivalent was greater than the global average value of 60 nGy/h and the natural background radiation value of 2.4 $mSvy^{-1}$.

KEYWORDS

Gamma ray spectrometry; radiogenic heat potential; crystalline basement rocks

Introduction

Gamma rays with no mass or electronic charge are emitted at different energy levels that correspond to the radioactive decay of particular radioisotopes. The relative abundance or concentration of these radioelements in soil and bedrock is estimated from the intensity of their emission peaks. However, only potassium, uranium and thorium decay series have radioisotopes that produce gamma rays of sufficient energy and intensity to be measured by gamma-ray spectrometry (IAEA 2003), because they are relatively abundant in the natural environment. These radionuclides occur in virtually all types of rocks and soils due to geochemical processes which have slowly recycled the crustal material to and from the earth's mantle. Thus, the "radioactive imprint" of rocks makes radiometric prospecting for lithological discrimination a useful tool (Lima et al. 2005; Frattini et al. 2006; Guagliardi et al. 2013).

These radioisotopes generate moderate amounts of heat (Costain et al. 1979; Waples 2001). The energy produced by the decay of these radioactive elements accounts for a large fraction, about 98%, of the heat flow at the surface of continents (Birch 1954; Clark and Ringwood 1964; Wasserburg et al. 1964; Sclater et al. 1980; Taylor and McLennan 1995; Jaupart and Mareschal 2004; Slagstad 2008; Holmberg et al. 2012). Areas of high heat production are increasingly being identified as possible targets for hot, dry-rock geothermal resources (Hasterok and Chapman 2011; Willmot et al. 2015). However, they also constitute a source of irradiation of the human body (UNSCEAR 2000; IAEA 2005). For instance, the accumulation of radionuclides through ingestion could have significant health effects such as bone cancer, leukaemia and increased blood pressure (Tettey-Larbi et al. 2013; Faanu et al. 2016).

Okene is geologically located within the crystalline basement complex of southwestern Nigeria, with abundant rock exposures that constrain the settlement pattern, mostly along the feet of the rocks. Thus, the inhabitants are exposed daily to uncontrolled gamma radiation outdoors. The use of the rock materials for both aesthetic and building construction also leads to exposure to radiation indoors. The intermittent power supply has also crippled both social and economic activities in the area, hence the need for an alternative energy source. Furthermore, alteration, tectonic activities (e.g. shearing and deformation of rocks), metamorphism and/or weathering have been recognised as important processes in modifying the redistribution of

CONTACT M. A. Adabanija maadabanija@lautech.edu.ng

these radioactive elements in rocks (Johnson 1979; Verdoya et al. 2001). The concentration of the radionuclides in the rocks therefore varies with local geological conditions (Xinwei et al. 2006). Hence, in this study, the background radiation level as well as the radiogenic potential of samples of the crystalline rock in the Okene (southwestern Nigeria) basement complex are investigated and appraised. The objectives are to: establish baseline information on the background radiation level of the area such that anthropogenic contamination can be easily detected and determined, determine the level of natural radioactivity associated with different rocks in the area, assess the suitability of the rocks for building and aesthetic construction in terms of the dose rates, assess the radiogenic heat potential of the rocks as an alternative energy source, and identify the controlling geological process(es) influencing the concentration of radionuclides in the rocks.

The main limitation of this study specifically in obtaining the radiogenic heat production is the ambiguity in representativeness of the samples collected. The samples were thought to be fresh but were collected near the surface and as such susceptible to water circulation in the near-surface environment, which could invariably lead to uranium depletion (Oversby 1976; Jaupart et al. 1981; Forster and Forster 2000), suggesting shallow and leached samples may not be representative of rocks from the same massif at greater depth. However, measurements of the heat production rate at outcrops has been established as an effective and valid proxy for rocks at depth (Willmot et al. 2015).

Geology of the study area

The study area is located between longitude 6°10′ and 6°19′E and latitude 7°30′ and 7°38′N (Figure 1). It lies geologically within the Precambrian basement rocks, in which a migmatite-gneiss complex rock is associated with series of metasedimentary rocks and older granite (Figure 2). The dominant lithological units in the study area are gneisses (which are regionally emplaced), ferruginous quartzites, granites, pegmatite and charnockite (Olade 1978; Fadare 1983; Annor and Freeth 1985; Adegbuyi and Olade 1990; Akinrinsola and Adekeye 1993; Dada et al. 1994). Both the crystalline basement and the metasedimentary cover are in places intruded by a suite of orogenic granites of Pan African age (600 Ma), known as the older granites (Ezepue and Odigi 1993; Odigi et al. 1993) to differentiate them from the much younger anorogenic granites of Jurassic age confined to the Jos plateau in central Nigeria. These rocks were subjected to multiple phases of deformation resulting in the development of faults and folds of which the Itakpe synform and Kuroko antiform are most prominent. However, minor folds suggest at least two phases of deformation, namely an early phase with east–west-trending axes and a later phase with northwest–southeast (NW–SE) axes (Annor and Freeth 1985). The proterozoic schist belts represent a supra-crustal cover of low-grade

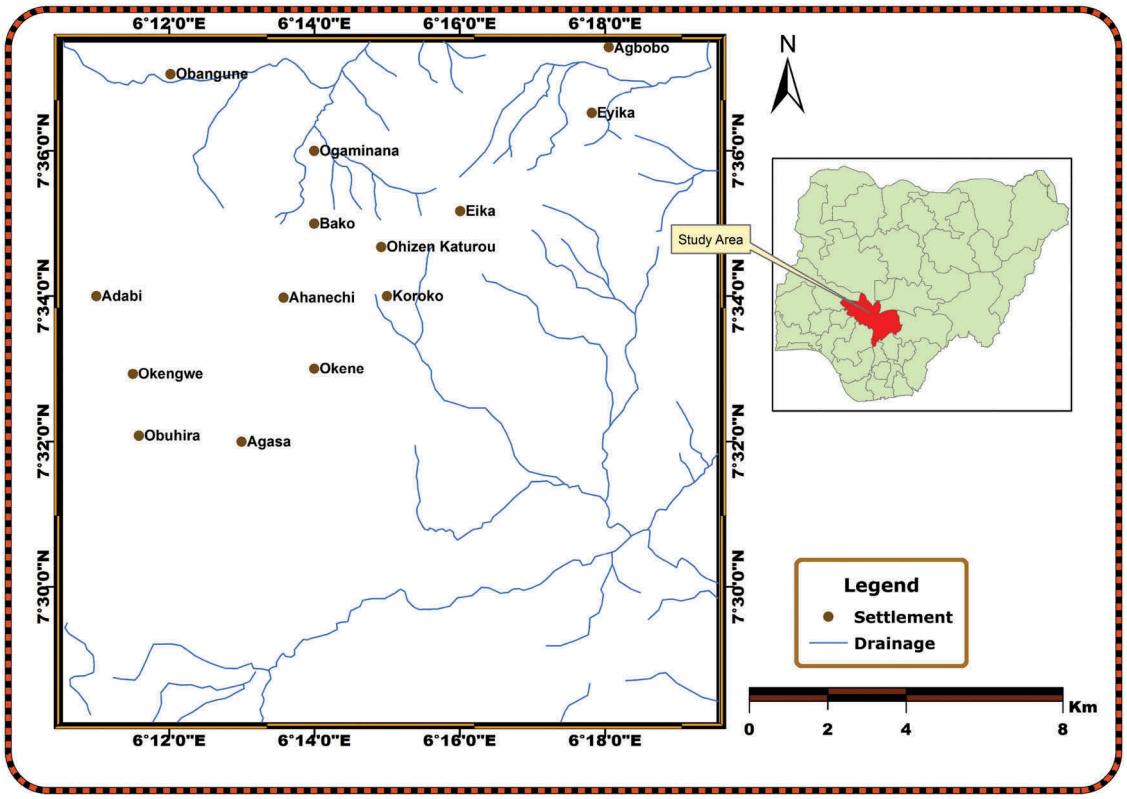

Figure 1. Location map of the study area.

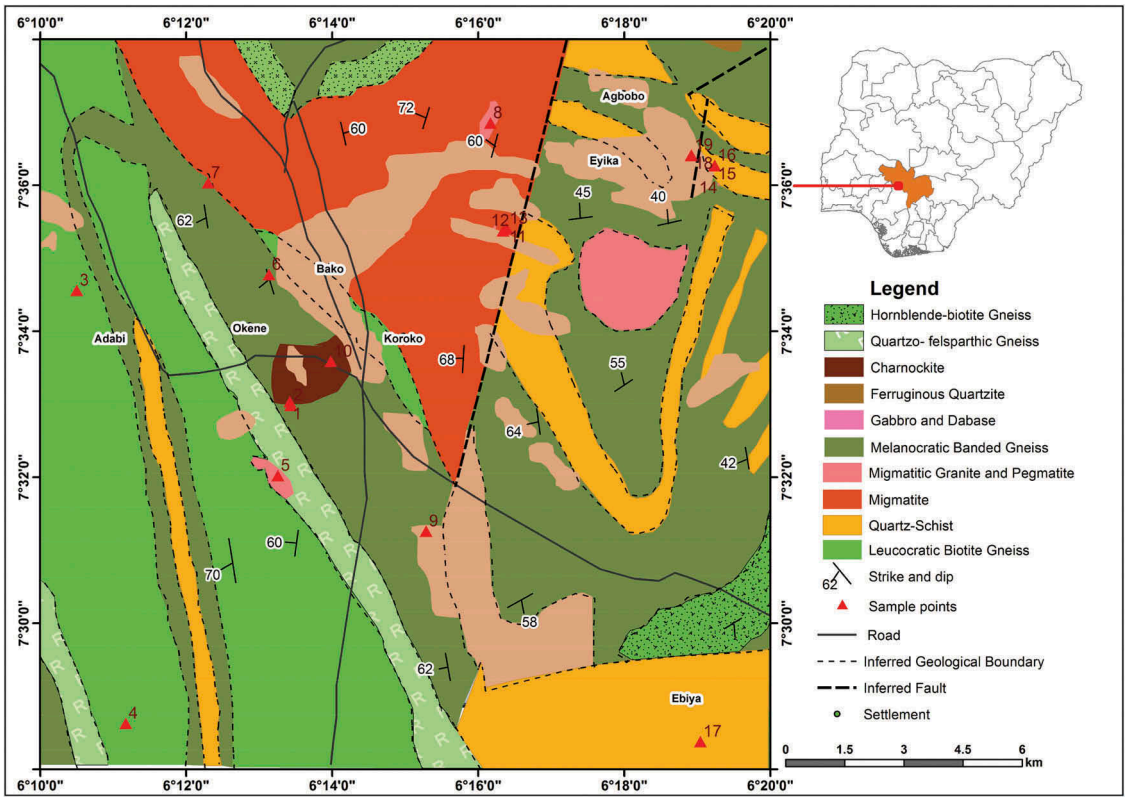

Figure 2. Geological map of part of the Okene area (adapted from Adegbuyi 1981).

metasediments and metavolcanics confined to linear but discontinuous belts that are steeply unfolded into the reactivated archean basement, gneissic-migmatitic (Olade and Elueze 1979; Adekoya 1993).

Climate, geomorphology, landform and drainage pattern of the study area

The Okene area is located climatically within forest savannah. The vegetation mainly comprises scattered trees and tall grass (Amigun et al. 2015). It has an annual rainfall of between 1100 and 1300 mm. The streams and springs around the study area are seasonal with a complex dendritic drainage network pattern (Figure 1). The numerous rivulets in the area are tributaries to the major rivers in the area: Osse, Osara and Omyi.

Materials and methods

Collection of samples

A total of 19 fresh rock samples of different lithology, comprising granite (5), charnockite (2), biotite granite (2), pegmatite (5), banded gneiss (3) and schist (2), were collected from the outcrops at different locations in the study area (Figure 1). The geographic coordinates of sampled rocks/locations were measured using a hand-held global positioning system GPSMAP® manufactured by Garmin, relative to the Minna Nigeria datum.

Sample preparation and laboratory analysis

Prior to sample measurement and analysis at the Centre for Energy Research and Development (CERD), Obafemi Awolowo University, Ile-Ife, Nigeria, the rock samples were pulverised into powder form and placed in a drying oven at a temperature of 60°C for 24 hours to ensure that any significant moisture was removed from the samples. To obtain uniform particle sizes, a 500-μm mesh was used to sieve the samples which were then weighed and transferred to 550-mL labeled Martinelli beakers and sealed to prevent Rn-223 leakage. Measurements were carried out on samples after about 30 days to allow the re-establishment of radioactive equilibrium between Rn-223 and its short-lived daughter products (Alnour et al. 2012a, 2012b). The gamma ray count was done at CERD using a Canberra S100 multi-channel analyser (MCA) with a voltage of 0.75 kV, for a duration of 36,000 seconds. The isotope K-40 emits gamma rays with an energy of 1.461 MeV, and hence the determination of the potassium was direct. The determination of both U-238 and Th-232 was indirect and hence based on the detection of the Bi-214 and Ti-208 radionuclide, respectively, which are corresponding members of the U-238 and Th-232 decay series, emitting respective energies of 1.764 and 2.615 MeV (Guagliardi et al. 2013).

Determination of radiogenic heat

The heat production rate of individual samples was calculated following Rybach (1988), based on the

samples' K, U and Th concentrations, and their density. The heat produced can be quantified in W kg^{-1}, as:

$$H = 10^{-11}(9.52[U] + 2.56[Th] + 3.48[K]) \quad (1)$$

where [U] and [Th] are the uranium and thorium concentrations in ppm and [K] is the potassium concentration in percent. The heat production per unit volume, A, is given by

$$A = \rho H \quad (2)$$

where ρ is the sample density.

For an average crustal density of 2700 kg m^{-3}, the heat production per unit volume A (in μWm^{-3}) was calculated as

$$A = 0.257[U] + 0.069[Th] + 0.094[K] \quad (3)$$

Determination of elemental concentration

The elemental concentrations of U-238 and Th-232 in ppm, and K-40 in percent (%), in the rock samples were computed using the expression

$$F_E = \frac{M_E.C}{\lambda_E.N_A.f_{AE}} \cdot \frac{1}{n}\sum_{i=1}^{n} A_i \quad (4)$$

where F_E is the fraction of element E in the sample, M_E is the atomic mass (kg mol^{-1}), λ_E is the decay constant (sec^{-1}) of the parent radioisotope, N_A is the Avogadro constant (6.023×10^{23} atoms mol^{-1}), f_{AE} is the fractional atomic abundance of Th-232, U-238 or K-40 in nature, C is a constant with a value of either 100 or 1,000,000 that converts the ratio of K-40 or U-238/Th-232 mass to soil mass in percentage or ppm, and A is the radiological concentration of K-40 (n = 1) or that of selected daughter radionuclides in the decay series of U-238 and Th-232 (n = 2).

Estimation of ambient gamma radiation dose rate

The external radiation dose rate in air absorbed by the general public living in the study area was estimated in nGy/h at 1 m height from different lithologies and was calculated from the following equation (UNSCEAR 2000) assuming that the contributions from other naturally occurring radionuclides and cosmic radiation at the locations were insignificant:

$$D(nGy/h) = 0.462A_{U-238} + 0.604A_{Th-232} + 0.0417A_{K-40} \quad (5)$$

where $A_{U\text{-}238}$, $A_{Th\text{-}232}$ and $A_{K\text{-}40}$ represent the activity concentrations of U-238, Th-232 and K-40 (in Bq/kg), respectively. The annual effective dose equivalent due to the absorbed dose rate in air was computed using 8760 hours for 1 year, an indoor occupancy factor of 0.8 and a conversion coefficient of 0.7, according to Equation (6):

$$E(Sv/y) = D(nGy/h) * 8760h/y * 0.8 * 0.7Sv/Gy * 10^{-6} \quad (6).$$

Results and discussion

The activity concentrations of each radionuclide in each rock sample are listed in Table 1. The gamma ray spectra associated with some of the sample rocks are depicted in Figure (3(a–c)). The concentrations of the radionuclides; in % for K-40 and ppm for U-238 and Th-232, as well as the equivalent radiogenic heat potential in Wm^{-3} based on different lithologies are as illustrated by box plots in Figures 4 and 9, respectively.

Table 1. Radionuclide concentrations in the basement rock samples, Okene area, southwestern Nigeria, using a Canberra S100 at a counting time of 36,000 seconds.

	Geographic coordinates		Concentration of radionuclides (Bq/kg)		
Rock samples	Longitude	Latitude	K-40	U-238	Th-232
Granite	6°13.418′E	7°33.007′N	1023.38	58.14	27.30
Charnockite	6°13.431′E	7°32.959′N	1198.56	43.42	19.69
Granite	6°10.501′E	7°34.534′N	415.25	16.24	12.99
Biotite granite	6°11.172′E	7°28.604′N	227.64	27.68	25.79
Pegmatite	6°13.255′E	7°31.998′N	1075.06	58.50	34.78
Banded gneiss	6°13.134′E	7°34.751′N	156.38	38.30	21.92
Banded gneiss	6°12.302′E	7°36.008′N	596.84	29.08	21.15
Pegmatite	6°16.166′E	7°36.828′N	701.87	20.52	26.33
Granite	6°15.286′E	7°31.236′N	498.94	29.24	28.52
Charnockite	6°13.981′E	7°33.563′N	941.16	15.29	20.05
Schist	6°16.385′E	7°35.384′N	843.92	40.82	5.09
Pegmatite	6°16.341′E	7°35.352′N	1526.00	31.46	19.79
Biotite granite	6°16.385′E	7°35.385′N	204.66	26.20	13.48
Pegmatite	6°19.237′E	7°36.245′N	1987.34	25.87	20.38
Pegmatite	6°19.237′E	7°36.245′N	1149.67	28.77	20.63
Granite	6°19.237′E	7°36.246′N	1579.35	28.47	23.91
Schist	6°19.040′E	7°28.353′N	369.73	40.29	34.34
Granite	6°18.919′E	7°36.382′N	412.41	17.11	21.74
Banded gneiss	6°18.919′E	7°36.390′N	824.25	31.50	44.28
Minimum			156.38	15.29	5.09
Maximum			1987.34	58.5	44.28
Mean			828.02	31.94	23.27
Median			824.25	29.08	21.74

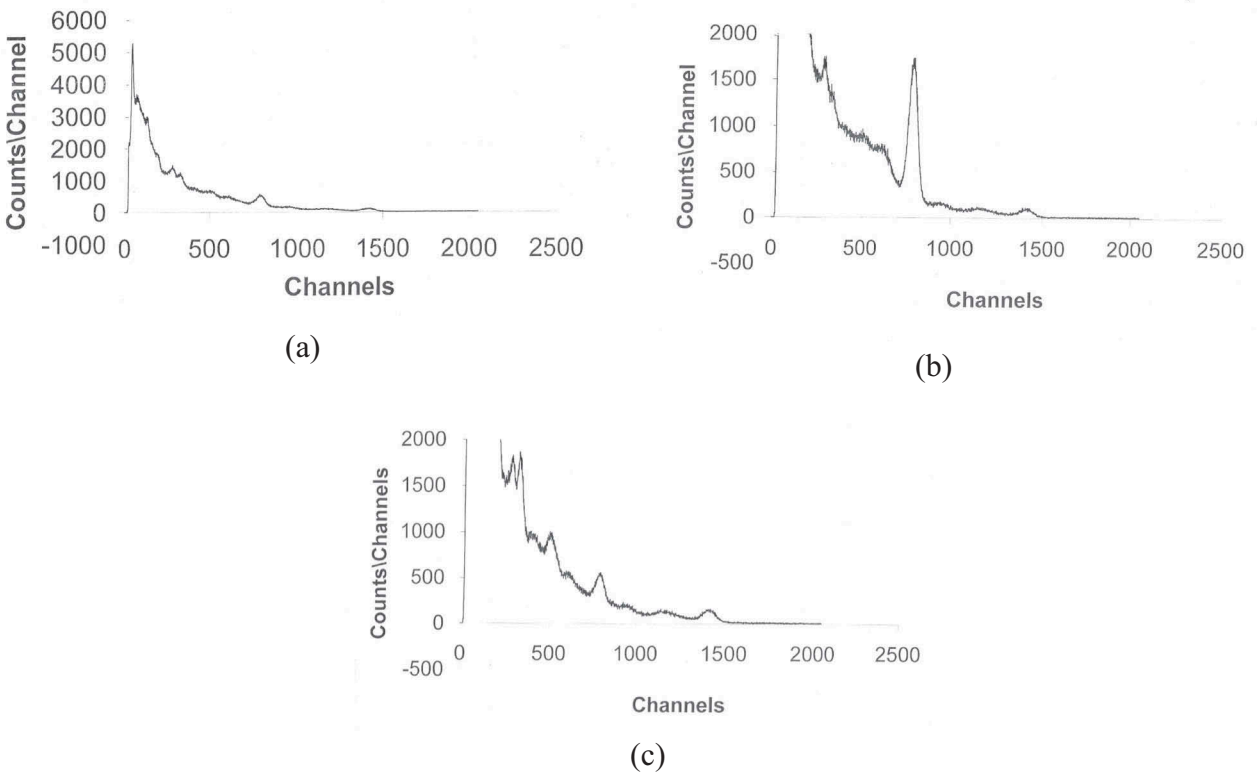

Figure 3. Gamma ray spectrum associated with some crystalline rock samples, Okene, southwestern Nigeria: (a) granite; (b) pegmatite; (c) schists.

Radioactivity level

The level of natural radioactivity in terms of the activity concentration of each naturally occurring radionuclide ranged between 156.38 and 1987.34 Bq/kg with a respective mean and median of 828.02 Bq/kg and 824.25 Bq/kg for K-40; a range of 15.29–58.5 Bq/kg with a mean of 31.94 Bq/kg and median of 29.08 Bq/kg for U-238; and a range of 5.09–44.28 Bq/kg with a mean and median of 23.27 Bq/kg and 21.74 Bq/kg, respectively (Table 1). These indicate the activity levels were in the order K-40 > U-238 > Th-232.

Elemental concentrations

K-40

The elemental concentration of K-40 ranged from 0.159 $\times 10^{-3}$% to 0.609 $\times 10^{-3}$% with a mean of 0.303 $\times 10^{-3}$% and median of 0.192 $\times 10^{-3}$% in granite; 0.271 $\times 10^{-3}$ – 0.766 $\times 10^{-3}$% with a respective mean and median of 0.496 $\times 10^{-3}$% and 0.443 $\times 10^{-3}$% in pegmatite; 0.363 $\times 10^{-3}$ – 0.462 $\times 10^{-3}$% with a mean of 0.413 $\times 10^{-3}$% in charnockite; 0.060 $\times 10^{-3}$ – 0.318 $\times 10^{-3}$% with a mean of 0.114 $\times 10^{-3}$% in banded gneiss; 0.143 $\times 10^{-3}$ – 0.325 $\times 10^{-3}$% in schist with a mean of 0.234 $\times 10^{-3}$%; and 0.079 $\times 10^{-3}$ – 0.088 $\times 10^{-3}$% with a mean of 0.084 $\times 10^{-3}$% in biotite granite (Figure 4(a)). Thus, the mean concentrations were in the order pegmatite > charnockite > granite > schist > banded gneiss > biotite granite. These suggest the amount of radioactive potassium (i.e. K-40) in the granite of the study area was much lower than the > 90% amount of potassium usually found in granite rocks (Hareyama et al. 2000). Moreover, the mean concentration of K-40 in the granite as well as the banded gneiss of the study area is high compared to Ikogosi/Nordic granite and Nordic gneiss, respectively (Table 2).

The spatial distribution shown in Figure 5(a) indicates the concentration of K-40 is very high – greater than 0.2 $\times 10^{-3}$ % in most parts of the study area, with notable concentration highs H1 and H2 having respective values of 0.55 $\times 10^{-3}$% and 0.45 $\times 10^{-3}$%. The concentration high H1 is flanked by the concentration low L of value 0.15 $\times 10^{-3}$% and the concentration high H2 northeastward and southwestward, respectively, indicating the concentration of K-40 initially increases from L to H1 and subsequently decreases southward, resulting in the lowest concentration value of 0.05 $\times 10^{-3}$% at the southwestern edge. The lowest concentration L_v is also notable towards the northwestern part of the area. The change in the K-40 level between anomaly H1 and L suggests lithological contacts (Ojala et al. 2007).

U-238

The concentration of U-238 was maximum in schist, ranging from 3.26 to 3.31 ppm with a mean of 3.29 ppm. In the other rock samples, its concentration varied between 1.32 and 4.71 ppm with a mean of

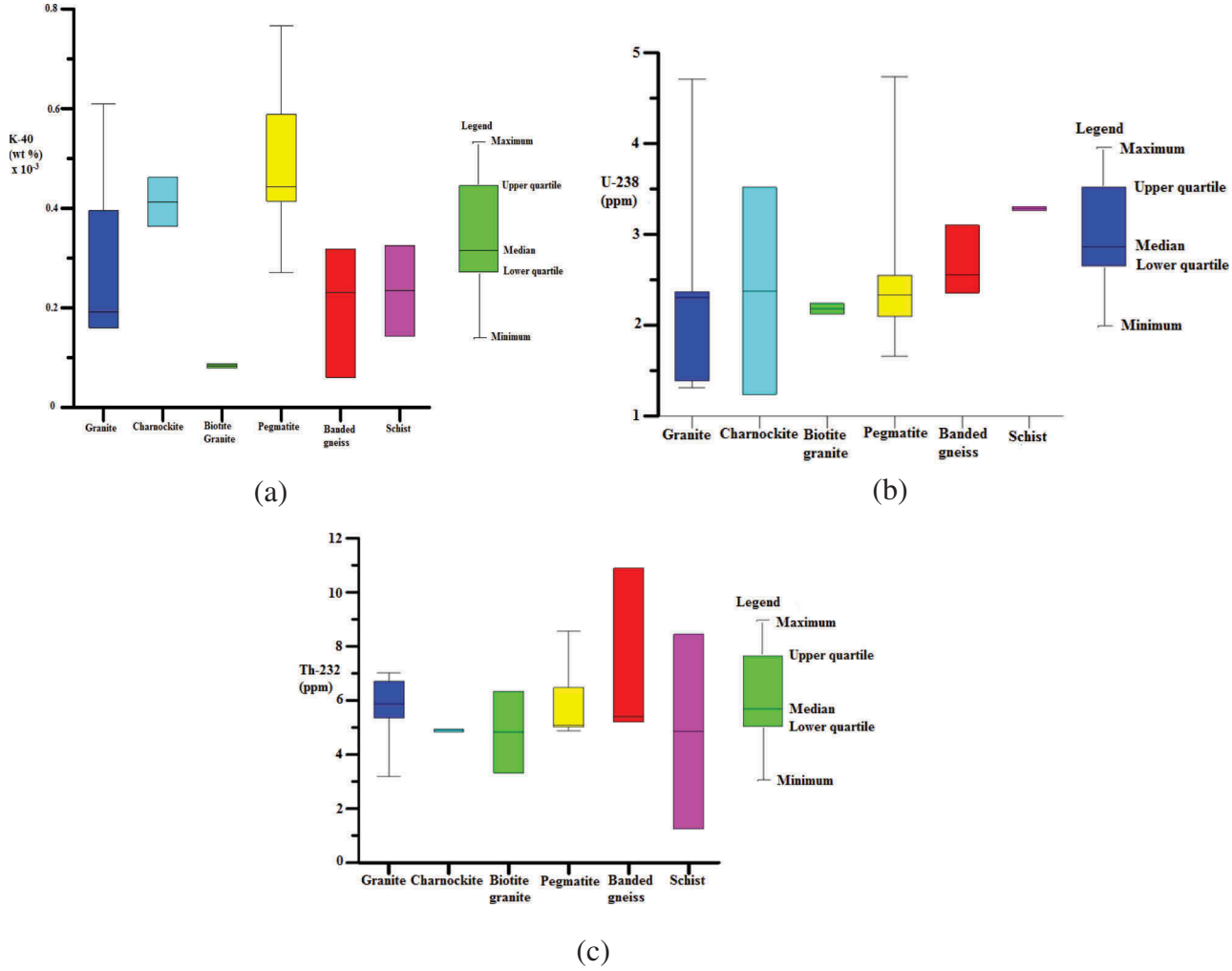

Figure 4. Variation in concentrations of radionuclides according to lithology: (a) K-40; (b) U-238; (c) Th-232.

2.42 ppm in granite; 1.24–3.52 ppm with a mean of 2.38 ppm in charnockite; 1.66–4.74 ppm with a mean of 2.68 ppm in pegmatite; 2.36–3.10 ppm with a mean of 2.67 ppm in banded gneiss; and 2.12–2.24 ppm in biotite granite with a mean of 2.18 ppm (Figure 4(b)). These suggest the concentrations were in the order schist > pegmatite > banded gneiss > granite > charnockite > biotite granite, and that they lie within 1–10 ppm for granite and clastic sediments of granitic origin (Maxwell et al. 2013). The concentrations of U-238 are above the upper crustal abundance of 2.8 ppm (Joshi et al. 2019) in all of the rock samples except biotite granite. Furthermore, the mean concentration of U-238 in the granite of the study area lies within the mean obtained for Nordic granite but is less than that of Ikogosi (Table 2).

Spatially, the concentration of U-238 is highest at H4 with a value of 4.8 ppm, and high at H5 having a value of 3.0 ppm, but low at L1 and L2 with respective values of 1.2 and 1.6 ppm (Figure 5(b)). The high and low U-238 concentrations occur alternately trending NE–SW, with high H4 and low L2 at the southwest and northeast ends, respectively, indicating anomalous distribution. This is exemplified by a decrease in concentration of U-238 outward from H4, southwestward, westward, northward and southward, forming a north–south trending ridge of concentration highs within 3.0–4.8 ppm. However, the concentration of U-238 increases northeastward and southeastward around lows L2 and L1, respectively. High U-238 contents have been observed in a weathered aplite dyke intersecting the granite (Trindade et al. 2013) indicating intrusion and-or contact. This suggests the alternating high and low concentration of U-238 from H4 through L1, H5 and L2 in a SW–NE direction can be attributed to intrusion.

Table 2. Comparison of average concentrations of radionuclides obtained in the Okene area, southwestern Nigeria, with those of Ikogosi and Nordic rocks.

Area	Rock type	K-40 (%) × 10^{-4}	Th-232 (ppm)	U-238 (ppm)
Okene*	Granite	3.03	5.63	2.42
	Gneiss	1.14	7.16	2.67
Nordic	Granite	0.39–1.93	295.2–369.0	3.24–28.35
	Gneiss	0.10–0.50	127.9–442.8	1.62–6.48
Ikogosi	Granite	0.22	61.40	6.61

*Current study.

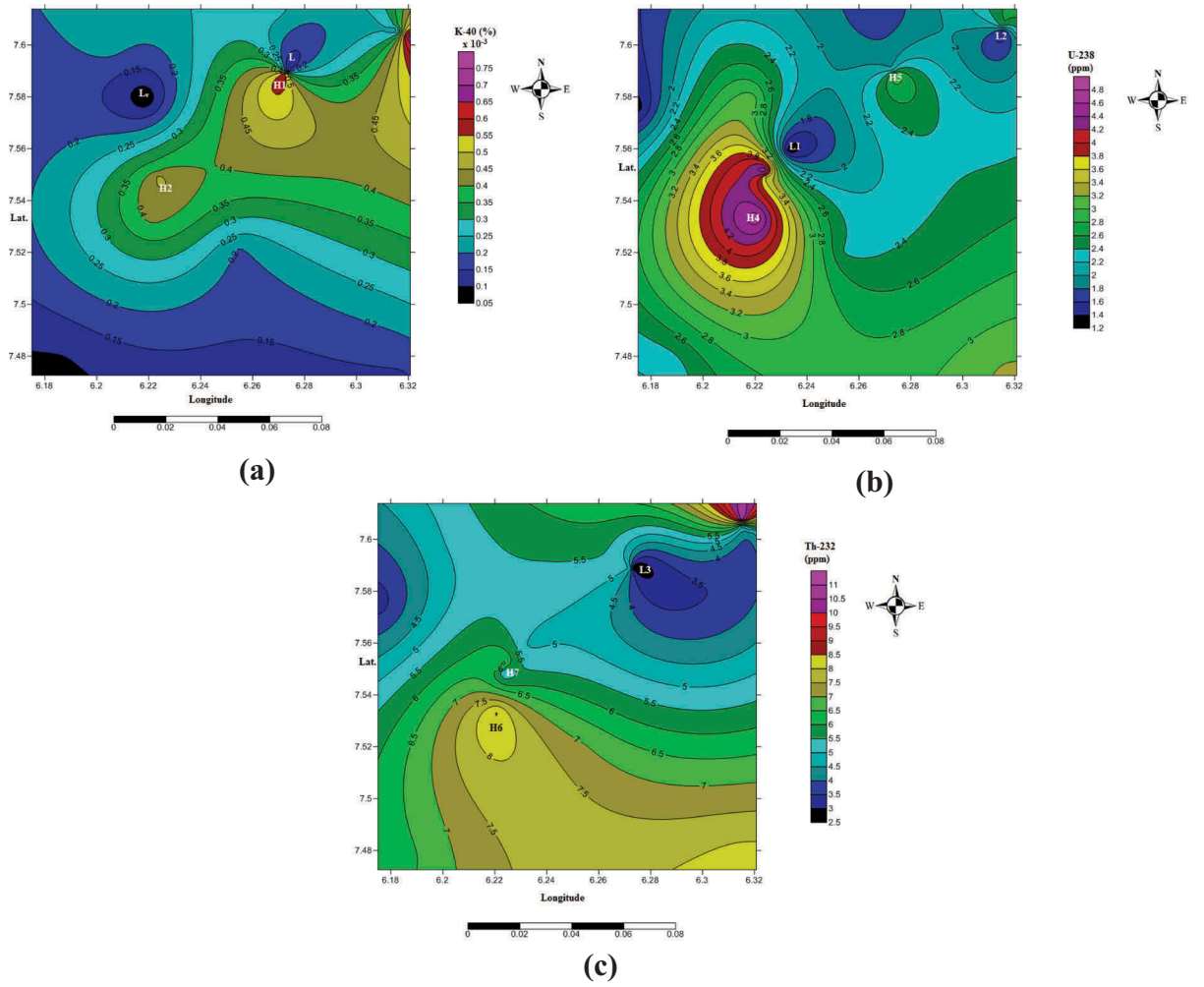

Figure 5. Spatial distribution of concentration of radionuclides: (a) K-40; (b) U-238; (c) Th-232

Th-232

The concentration of Th-232 varied from 3.20 to 7.02 ppm with a mean of 5.63 ppm in granite; 4.84 to 4.93 ppm with a mean of 4.89 ppm in charnockite; 3.32 to 6.34 ppm with a mean of 4.83 ppm in biotite granite; 4.87 to 8.56 ppm with an approximate mean of 6.02 ppm in pegmatite; 5.20 to 10.89 ppm with a mean of 7.16 ppm in banded gneiss; and 1.25 to 8.45 ppm in schist with a mean of 4.85 ppm (Figure 4(c)). These suggest the mean concentrations of Th-232 were in the order banded gneiss > pegmatite > granite > charnockite > schist > biotite granite. Furthermore, the mean concentration of Th-232 obtained for granite in the study area is very low compared to Nordic and Ikogosi granite (Table 2). However, the concentrations of Th-232 are below the crustal abundance of 10.7 ppm (Joshi et al. 2019) in all the rock samples except banded gneiss.

The spatial distribution in Figure 5(c) indicates concentration highs of Th-232 at H6 and H7 with respective concentrations of of 8.0 ppm and 5.0 ppm, but a low at L3 with a value of 2.5 ppm. The elemental concentration of Th-232 decreases away from highs H6 through H7 northeastward, reach a minimum at L3 and then increase northward and farther northeastward where a very high concentration value of 11.0 ppm was recorded.

Enrichment and depletion of radionuclides

Th-232/U-238

The Th-232/U-238 ratio ranged from 1.43 to 3.86 with an average of 2.65 in granite; between 1.81 and 3.90 with a mean of 2.44 in pegmatite; between 1.74 and 4.27 with a mean of 2.74 in banded gneiss; between 1.38 and 3.98 with a mean of 2.68 in charnockite; between 0.38 and 2.59 with a mean of 1.49 in schist; and between 1.56 and 2.83 with a mean of 2.20 in biotite granite (Table 3). These values suggest depletion of U-238 relative to Th-232 in all the samples except in one of the schist samples which could be regarded as least depleted, whilst banded gneiss was most depleted. The mean ratio obtained for granite is greater than continental crust values of 1.2 and 1.8 for

Table 3. Relative enrichment and depletion of the radionuclides in crystalline basement rocks, Okene area, southwestern Nigeria.

	Elemental concentration ratio of radionuclides								
	Th-232/U-238			*K-40/U-238*			*K-40/Th-232*		
Rock types	*Min.*	*Max.*	*Mean*	*Min.*	*Max.*	*Mean*	*Min.*	*Max*	*Mean*
Granite	1.43	3.86	2.65	0.81	2.64	1.33	0.27	1.04	0.54
Pegmatite	1.81	3.90	2.44	0.87	3.65	2.07	0.41	1.53	0.90
Banded gneiss	1.74	4.27	2.74	0.19	1.24	0.81	0.11	0.44	0.28
Biotite granite	1.56	2.83	2.20	0.37	0.39	0.38	0.14	0.24	0.19
Charnockite	1.38	3.98	2.68	1.31	2.93	2.12	0.74	0.95	0.84
Schist	0.38	2.59	1.48	0.44	0.98	0.71	0.17	2.60	1.38

granite given by Eisenbud and Gesell (1997) but lower than the value of 3.2 obtained for granite from Szklarska Poreba (Plewa and Plewa 1992). Generally, however, Th/U concentration ratios in rocks in the current study are within those of crystalline rocks (1.5–3.2) of the Iera block (Malczewski et al. 2005).

Spatially, the Th-232/U-238 ratio map (Figure 6(a)) indicates two categories of high and low Th-232/U-238 ratios, H1-1 and H1-2, and L1-1 and L1-2, respectively, with corresponding values of 3.8 and 3.0, and 1.6 and 0.6. The configuration of the high and low Th-232/U-238 ratios indicates alternation between H1-1 and L1-1 in a NW–SE direction, with H1-1 and L1-1 at the southeast and northwest ends, respectively. These indicate alternating enrichment and depletion (but in a specific order: enrichment–depletion–enrichment), of Th-232 relative to U-238 from the northwestern to the southeastern part of the study area. The same feature also plays out in a SW–NE direction except the alternation involves admixtures of H1-1, H1-2, L1-1 and L1-2 with the configuration H1-1, L1-1 (slightly dislodged northwestward and southeastward), H1-2 (slightly dislocated northwestward), L1-2 and H1-2. The alternation here indicates depletion–enrichment–depletion–enrichment of Th-232 relative to U-238. Likewise, in a WSW-ENE direction, enrichment and depletion alternate in the order depletion–enrichment–depletion, with highs and lows in the configuration H1-1 – L1-1 – H1-2 – L1-2.

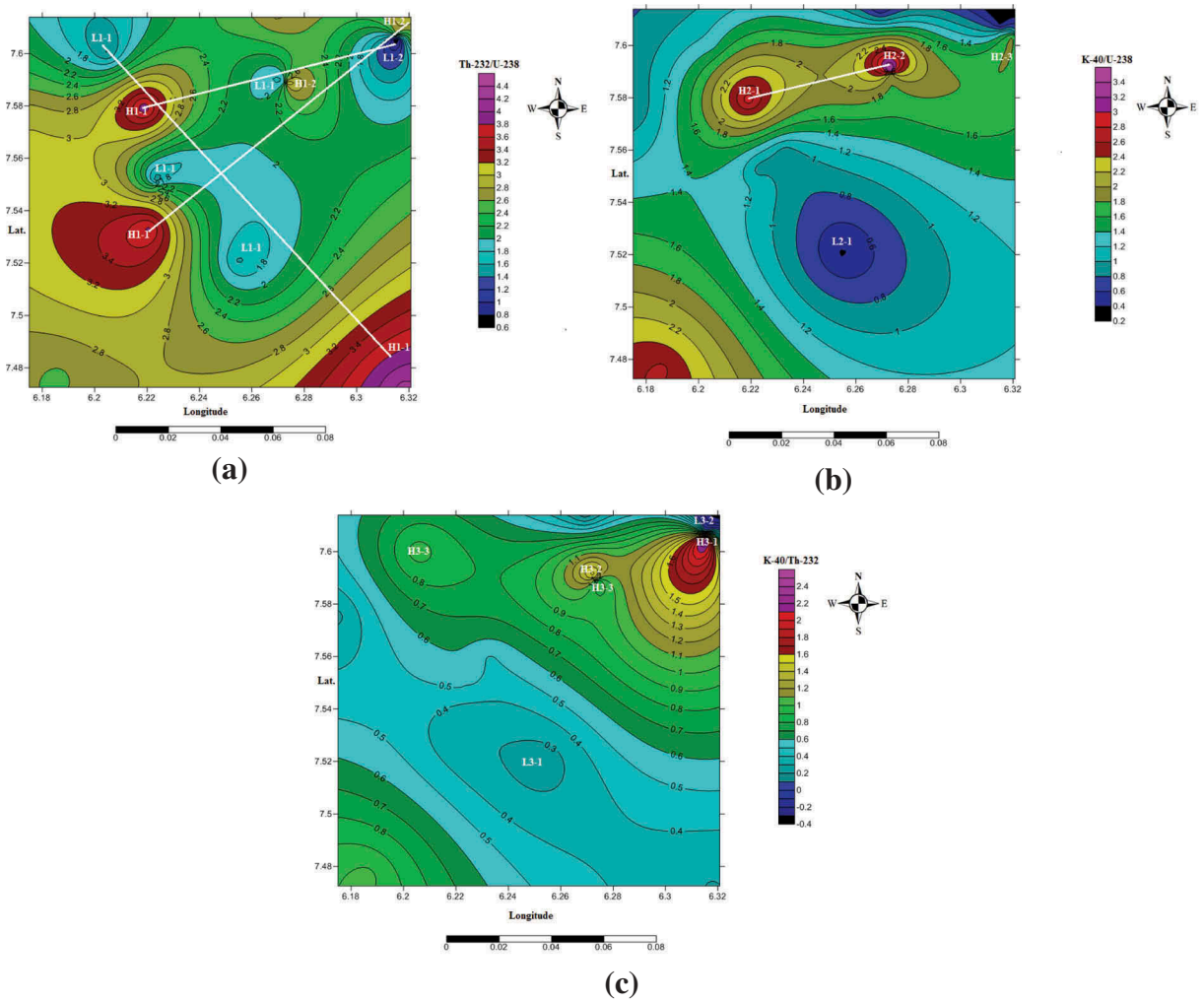

Figure 6.. Ratio map of (a) Th-232/U-238; (b) K-40/U-238; (c) K-40/Th-232.

Anomalies in the Th-232/U-238 ratio could be due to shearing, metamorphism and/or weathering of the investigated rocks (Banerjee et al. 2011). Furthermore, thorium enrichment based on the Th-232/U-238 ratio has been attributed to remobilisation of radioisotopes due to intense mylonitisation and metamorphism (Mukherjee et al. 2007; Joshi et al. 2019). Based thereon, alternating enrichment and depletion along NE–SW, NW–SE and WSW-ENE axes, illustrated by a white line in Figure 6(a), indicates remobilisation of Th-232 and U-238, implying metamorphism along the respective axes and suggesting deformation (Brodie and Rutter 1985) as a result of the inter-relationship between deformation and metamorphism. These are corroborated by folds along the WSW-ENE and NW–SE (Figure 2), while the NE–SW is exemplified by the intrusion of both the crystalline basement and metasedimentary by a suite of Pan African orogenic granites (Ezepue and Odigi 1993; Odigi et al. 1993). Furthermore, multiple phases of deformation of the rocks exist in the area (Annor and Freeth 1985). However, while at least two phases of deformation – an early phase with an E–W trending axis, and a later phase with a NW–SE axis – were recognised and established by Annor and Freeth (1985), evidence from the current study based on the Th-232/U-238 ratio map indicates three phases of deformation along NW–SE, NE–SW and WSW-ENE axes.

K-40/U-238

The computed mean K/U ratio (Table 3) suggests two main categories, namely depletion of U-238 relative to K-40 as exemplified by granite (least depleted), pegmatite and charnockite (most depleted); and enrichment of U-238 relative to K-40 as indicated by biotite granite (most enriched), schist and banded gneiss (least enriched).

The K-40/U-238 ratio map in Figure 6(b) indicates highs H2-1, H2-2 and H2-3 of values 2.8, 3.2 and 1.8, respectively, as well as low L2-1 with a value of 0.2. The ratio increases outwards around L2-1 at south central in NW–SE and NE–SW, but subsequently decreases from H2-1, H2-2 and H2-3. These indicate enrichment of K-40 relative to U-238 southwestward and southeastward but depletion northeastward and northwestward.

Enrichment of potassium is controlled mainly by syn- to post-magmatic processes during crystallisation and alteration of potassium feldspar and biotite minerals (De Capitani et al. 2007). The K/U ratio has also been recognised as capable of providing information about the relative depletion or enrichment of uranium with respect to potassium, which could be due to shearing, metamorphism and/or weathering of the investigated rocks (Banerjee et al. 2011). Based thereon, the anomalously high K-40/U-238 ratios at H2-1 and H2-2 enclosed in a ring along a WSW-ENE axis and connected by the white line in Figure 6(b) could be due to metamorphism. This further corroborates the existence of deformation along WSW-ENE axis as revealed by the Th-232/U-238 ratio map (Figure 6(a)) and the fold along WSW-ENE (Figure 2). Consequently, the anomalously low K-40/U-238 ratio L2-1 located southward of the anomalously high K-40/U238 ratios H2-1 and H2-2 trending WSW-ENE could be regarded as a shear zone. Furthermore, the resistes-like high K-40/U-238 ratio H2-3 also occurs in the NEE part of the study area. This could mean residual material left at the site melted during the in-situ production of granite through intense metamorphism and could be subjected to further investigation through whole-rock geochemical analysis.

K-40/Th-232

The computed mean ratio of K/Th ranged from 0.19 to 1.38 across all lithologies (Table 3), suggesting the enrichment of Th-232 relative to K-40 for all lithologies except schist (the ratio of which was greater than unity, indicating depletion of Th-232 relative to K-40). The enrichment of Th-232 relative to K-40 was in the order biotite granite > banded gneiss > granite > charnockite > pegmatite, while the enrichment of K-40 relative to Th-232 was in the order schist > pegmatite > charnockite > granite > banded gneiss > biotite granite.

The K-40/Th-232 ratio map (Figure 6(c)) indicates high K-40/Th-232 anomalies H3-1, H3-2 and H3-3 with values of 2.4, 1.5 and 0.9, respectively. There are also low K-40/Th-232 anomalies L3-1 and L3-2, with values of 0.3 and −0.2, respectively. Generally, however, there is a low K-40/Th-232 ratio along a NW–SE trend, about which it increases northeastward and southwestward, indicating enrichment of K-40 relative to Th-232 in these directions. Thus, the low anomaly along the NW–SE marks the boundary between two regions of high K-40/Th-232 anomalies.

Thorium enrichment generally does not accompany potassium during hydrothermal alteration processes, and as such its ratios to potassium are capable of providing a distinction between potassium associated with alteration and anomalies related to normal lithological variations (Galbraith and Saunders 1983). Thus, anomaly H3-1 in the east of the northeastern (NEE) part of the study area indicates alteration or pegmatite. Compared with the geological map (Figure 2), pegmatite (Sample 15) is found at NEE and in the central northeast (Sample 12), coinciding with anomaly H3-2. This important correlation of a high K-40/Th-232 ratio (low Th-232/K-40 ratio) with many alteration processes is evident in various studies worldwide (Shives et al. 1997; Ojala et al. 2007). Thus, the low anomaly L3-1 as well as the relatively low K-40/Th-232 along the NW–SE axis indicates lithological contacts or changes in the alteration style or type (Ojala et al. 2007). Comparison with the

geological map (Figure 2) suggests the low anomaly could be attributed to a change in alteration style as the anomaly marks the transition between two regions of high K-40/Th-232 to the northeast and southwest. Furthermore, the occurrence of migmatite-gneiss in the study area (Figure 2) suggests that slight changes in levels and K-40/Th-232 ratios could be used to detect the lithological contacts (Ojala et al. 2007). These are corroborated by the contact between anomalies H3-2 and H3-3 corresponding to sample 12 (pegmatite) and sample 11 (schist), respectively, on the geological map (Figure 2). This coincides with and further establishes the contact between anomalies H1 and L revealed by the K-40 spatial distribution map (Figure 5(a)) to be lithological.

Absorbed dose rate and annual effective dose equivalent

The measured average ambient gamma radiation dose rates in air at approximately 1 m height from different lithologies in the study area are as shown in Figure 7. The highest gamma radiation was emitted by pegmatite and ranged from 54.65 to 107.13 nGy/h with a mean of 83.69 nGy/h, which is significantly higher than the global average value of 60 nGy/h (UNSCEAR 2000). The lowest gamma radiation was from biotite granite, and varied between 28.78 and 37.86 nGy/h with a mean of 33.32 nGy/h. Thus, the mean gamma radiation emitted on the basis of lithology is in the order pegmatite > charnockite > granite > banded gneiss > biotite granite, suggesting its corroboration with the order of concentration of K-40 on a lithological basis.

On a radionuclide basis, the contribution due to U-238 is highest relative to other radionuclides in biotite granite with an absorbed dose range of 12.1 to 12.79 nGy/h and a mean absorbed dose of 12.45 nGy/h (Figure 7); it contributed an overall mean gamma radiation of 14.76 nGy/h, amounting to 23% of the global mean dose of the study area (Figure 8). However, K-40 was the most dominant source of gamma radiation in all lithologies except biotite granite (Figure 7) and hence was most responsible for gamma irradiation, as exemplified by the highest mean dose of 34.53 nGy/h contributing 55% of the overall average of the study area (much more than the combined mean due to U-238 and Th-232; see Figure 8). Thus, the overall average gamma radiation due to different lithologies in the area was 63.35 nGy/h (Figure 8), corresponding to an annual effective dose equivalent of 3.11 $mSvy^{-1}$ which is greater than the global average value of 60 nGy/h and the natural background radiation value of 2.4 $mSvy^{-1}$ (IAEA 1996). Hence, the gamma radiation may have an impact outdoors in the locality, and indoors when the rocks are used as building material.

Heat production and lithology

The radiogenic heat for each lithology, along with the minimum and maximum values and the 25th, 50^{th} (median) and 75th percentiles, is depicted in Figure 9. It indicates banded gneiss has the highest

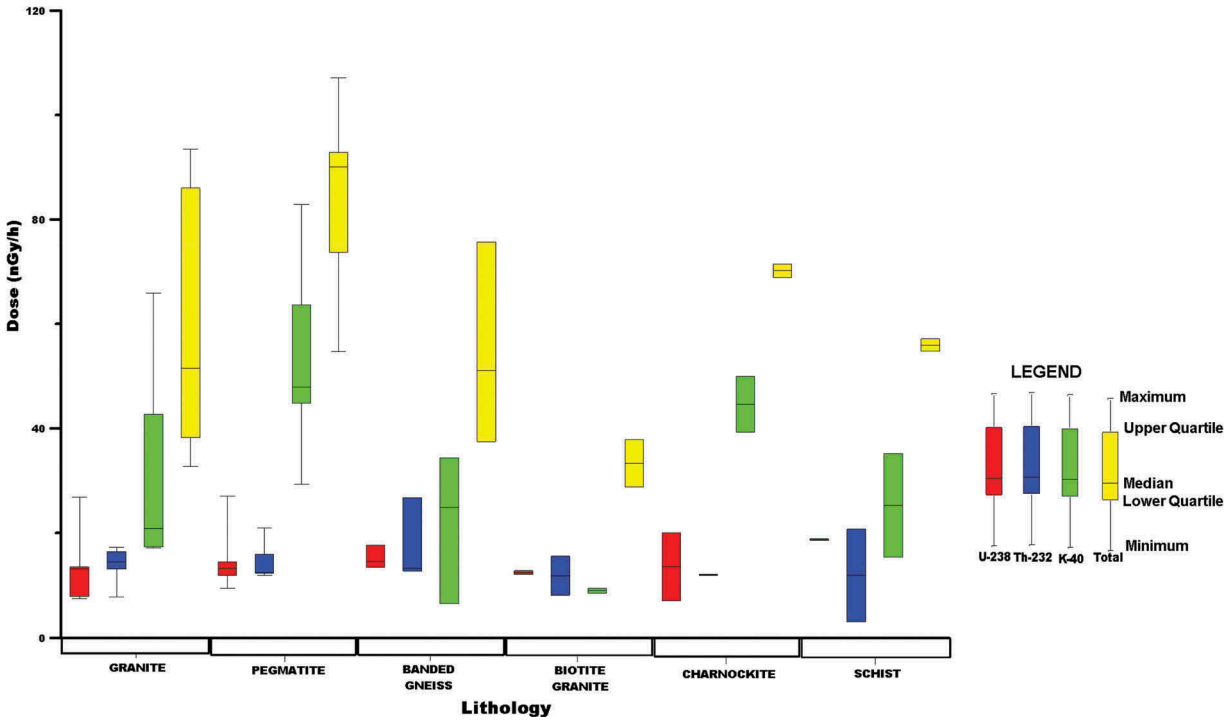

Figure 7.. Gamma radiation-lithology/radionuclide plots, Okene, southwestern Nigeria.

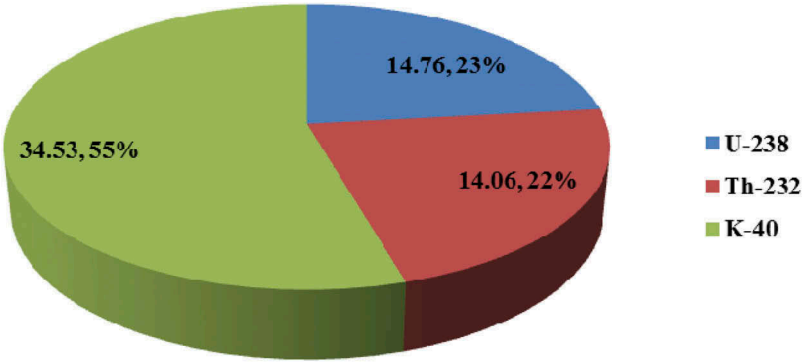

Figure 8. Percentage distribution of gamma radiation (nGy/h) by the radionuclides.

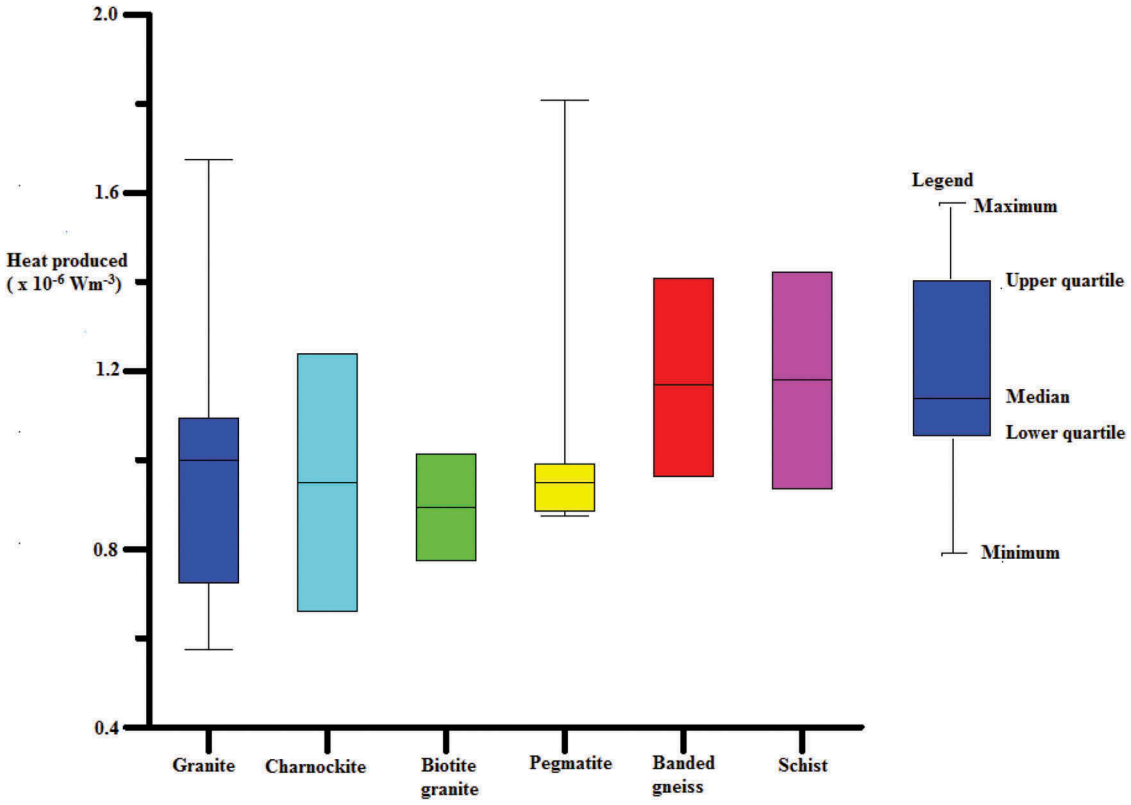

Figure 9. Radiogenic heat produced by lithology.

potential, ranging between 0.964 and 1.407 μWm^{-3} with a median of 0.964 μWm^{-3}, whilst biotite granite has the lowest potential, varying from 0.774 to 1.014 μWm^{-3} with a median heat generation capacity of 0.894 μWm^{-3}. Generally, the radiogenic heat production is in the order banded gneiss > schist > pegmatite > granite > charnockite > biotite granite. However, to expand the discussion of heat production and its dependence on lithology, the samples were sub-divided into five lithological groups (Table 4) based on Olade (1978), namely meta-sedimentary (schist); granodiorite-tonalite gneiss (banded gneiss); granitoids (charnockite); pegmatite and granodioritic/granitic rocks (granite and biotite granite). The granitoid group yields the lowest heat production with an average of 0.949 $\mu W/m^3$; the granodioritic/granite and pegmatite groups yielded intermediate heat production with averages of

Table 4. Radiogenic heat production based on lithology group in the Okene area, southwestern Nigeria.

Lithological group	No. of samples	Mean heat produced (μWm^{-3})	Median heat produced (μWm^{-3})
Meta-sedimentary	2	1.179	1.179
Granodiorite-tonalitic gneiss	3	1.180	0.964
Granitoids	2	0.949	0.949
Pegmatite	5	1.101	0.949
Granodioritic/granitic	7	0.979	0.999

0.979 and 1.101 μW/m^3, respectively; and the metasedimentary and granodiorite-tonalitic gneiss groups had the highest heat production with averages of 1.179 μW/m^3 and 1.180 μW/m^3, respectively, indicating radiogenic heat production varied with lithology. These suggest the temperatures were in the order granodiorite-tonalitic gneiss > metasedimentary > pegmatite > granodioritic/granitic > granitoids in the study area. Hence, variation in internal heat production may have important implications for temperature-dependent crustal processes such as metamorphism, magmatism and deformation (Bea et al. 2003; Andreoli et al. 2006; Sandiford and McLaren 2006; Slagstad 2008).

Conclusion

The background gamma radiation and radiogenic heat potential of Precambrian basement rocks in a crystalline basement complex of southwestern Nigeria were established. The mean concentrations of radionuclides were in the order pegmatite > charnockite > granite > schist > banded gneiss > biotite granite for K-40; schist > pegmatite > banded gneiss > granite > charnockite > biotite granite for U-238; and banded gneiss > pegmatite > granite > charnockite > schist > biotite granite for Th-232. However, while the concentrations of U-238 are higher than the upper crustal abundance of 2.8 ppm in all the rock samples except biotite granite, the concentrations of Th-232 are below the crustal abundance of 10.7 ppm in all the rock samples except banded gneiss.

The mean gamma radiation emitted on a lithological basis was in the order pegmatite > charnockite > granite > schist > banded gneiss > biotite granite, yielding an overall mean dose of 63.35 nGy/h corresponding to 3.11 mSvy^{-1} annual effective dose equivalent. This is considered high compared with the global average value of 60 nGy/h and the natural background radiation of 2.4 mSvy^{-1}. These values indicate the gamma radiation emanating from the rocks may have an impact on the inhabitants of the area, either outdoors or indoors when the rocks are used as building material and-or decorations.

The mean gamma radiation contributed by the radionuclides ranged between 14.06 and 34.53 nGy/h, with the highest contribution of 55% attributed to K-40 and representing much more than the combined mean due to U-238 and Th-232. These exemplified the dominance of K-40 as the most abundant of the naturally occurring radionuclides in the studied area.

The computed radiogenic heat potential indicated banded gneiss has the highest potential, ranging between 0.964 and 1.407 μWm^{-3} with a median of 0.964 μWm^{-3}, whilst biotite granite has the lowest potential, varying from 0.774 to 1.014 μWm^{-3} with a median heat production capacity of 0.894 μWm^{-3}.

The alternating enrichment and depletion along NE–SW, NW–SE and WSW-ENE axes as revealed by the Th-232/U-238 ratio map, and along the WSW-ENE axis as revealed by the K-40/U238 ratio map, indicate remobilisation of the radionuclides due to metamorphism along the respective axes. The high K-40/Th-232 ratio anomaly in the NEE part of the study area revealed by the K-40/Th-232 ratio map indicates alteration, while the low K-40/Th-232 ratio anomaly along the NW–SE axis indicates changes in the alteration style. These implicate metamorphism and alteration as the controlling geological processes influencing the redistribution of radionuclide concentrations in the rocks of the area.

The baseline information on the background radiation level as well as other valuable findings of the current study could serve as a veritable checklist for the Nigeria Atomic Energy Commission in advocating for the 4800-MW nuclear power plant site at Geregu, via Okene, the study area. Further research work involving the evaluation of whole-rock geochemical data to investigate the relationship between major/trace elements and natural radioactivity is strongly recommended, working towards a reconstruction of the geology and mineralogy of the studied area.

Acknowledgments

The authors are grateful to the National Research Institute of Astronomy and Geophysics for generous support for the publication of the research article at no cost.

Disclosure statement

No potential conflict of interest was reported by the authors.

ORCID

M. A. Adabanija http://orcid.org/0000-0002-3737-0350

References

Adegbuyi O 1981. Petrographic and geochemical study of Itakpe ridge iron deposit, Okene Nigeria in relation to ore genesis. *Unpublished Master of Science thesis*, Department of Geology, University of Ibadan, Ibadan Nigeria.

Adegbuyi O and Olade MA 1990. The Precambrian Itakpe iron ore deposit in central Nigeria. In: Ancient banded iron formations, *Theophrastus publications*, S. A. Athens Greece, 105-118.

Adekoya JA 1993. Proterozoic Maru and Birni-Gwari banded iron formations northwestern Nigeria. *Journ. of Mining & Geology*, 29(1): 63–76.

Akinrinsola EO and Adekeye JID 1993. A geostatistical ore reserve estimation of the Itakpe iron ore deposit Okene Nigeria. *Journ. of Mining & Geology*, 29(1): 19–25.

Alnour AI, Ibrahim N and Hossain I 2012a. Concentration of ^{214}Pb, ^{214}Bi in ^{238}U series and ^{208}Tl, ^{228}Ac in ^{232}Th series in granite rock in (Kadugli) Sudan. *Indian J. Pure Appl. Phys.* 50:285–682.

Alnour AI, Wagiran H, Ibrahim N, Laili Z, Omar M, Hamzah S and Bello YI 2012b. Natural radioactivity measurements in the granite rock of quarry sites, Johor, Malaysia. *Radiat. Phys. Chem*. 81: 1842–1847.

Amigun JO, Faruwa RA and Komolafe AA 2015. Integrated Landsat Imagery and Geophysical Exploration for Groundwater Potential Evaluation of Okene and Its Environs, Southwestern Nigeria. *International Journal of Geosciences*, 6:209–229.

Andreoli MAG, Hart RJ, Ashwal LD and Coetzee H 2006. Correlations between U, Th content and metamorphic grade in the Western Namaqualand Belt, South Africa, with implications for radioactive heating of the crust. *Journal of Petrology*, 47(6): 1095–1118.

Annor AE and Freeth SJ 1985. Thermotectonic evolution of the basement complex around Okene Nigeria with special reference to deformation mechanism. *Precamb. Res*. 28: 269–281

Banerjee KS, Guin R, Gutierrez-Villanueva JL, Charro ME and Sengupta D 2011. Variation in U-238 and Th-232 enrichment in U-mineralised zone and geological controls on their spatial distribution, Singhbhum Shear Zone of India. *Environ Earth Sci*

Bea F, Montero P and Zinger T 2003. The Nature, Origin, and Thermal Influence of the Granite Source Layer of Central Iberia, *The Journal of Geology*, 111: 579–595.

Birch F 1954. Heat from radioactivity. In Nuclear Geology (ed. H. Faul). Wiley, pp. 148–174.

Brown GC and Mussett AE 1993. The Inaccessible Earth: An integrated view to its structure and composition (2nd ed.), *Chapman & Hall*, London.

Clark SP Jr. and Ringwood AE 1964. Density distribution and constitution of the mantle. *Rev. Geophys*. 2: 35.

Costain JK, Glover L and Sinha AK 1979. Low- temperature geothermal resource potential of the eastern United States; Transactions, American Geophysical Union, G1, No. 1

Dada SS, Birck JL, Lancelot JR and Rahaman MA 1994. Archean magmatic-gneiss complex of north central Nigeria, its geochemistry, petrogenesis and crustal evolution. In: 16th international colloq. of Africa geology, Mbabane Swaziland. Geol. Surv. Mines Dept. Abstr 1, 77-102.

De Capitani L, Carnevale M and Fumagali M 2007. Gamma ray spectroscopy determination of radioactive elements in late-Hercynian plutonic rocks of Val Biandino and Val trompia (Lombardia, Italy. *Period Mineral* 76: 25–39

Eisenbud M and Gesell T 1997. Environmental Radioactivity from Natural, Industrial and Military Sources. Acad. press, San Diego, CA pp. 134–200.

Ezepue MC and Odigi MI 1993. Schistose rocks from Okene-Lokoja area, Southwestern Nigeria. *Journ. of Mining & Geology*, 30(1): 1–10.

Faanu A, Adukpo OK, Tettey-Larbi L, Lawluvi H, Kpeglo DO, Darko EO, Emi-Reynolds G, Awudu RA, Kansaana C, Amoah PA, Efa AO, Ibrahim AD, Agyeman B, Kpodzro R and Agyeman L 2016. Natural radioactivity levels in soils, rocks and water at a mining concession of Perseus gold mine and surrounding towns in Central region of Ghana. *SpringerPlus* 5: 98–113

Brodie KH and Rutter EH 1985. On the relationship between deformation and Metamorphism, with Special Reference to the Behaviour of Basic Rocks. In: Thompson AB, Rubie DC (eds) Metamorphic Reactions. *Advances in Physical Geochemistry*, 4.

Fadare VO 1983. Iron Ore Formation—The Okene-Ajaokuta-Lokoja Areas of Kogi State. A Potential Supply Base for Steel Plant at Ajaokuta. *Journal of Mining and Geology*, 20:209–214

Forster A and Forster H-J 2000. Crustal composition and mantle heat flow: implications from surface heat flow and radiogenic heat production in the Variscan Erzgebirge (Germany). *J. Geophys. Res*. 105: 27917–27938.

Frattini P, De Vivo B, Lima A and Cicchella D 2006. Elemental and gamma-ray surveys in the volcanic soils of Ischia Island (Italy). *Geochemistry: Exploration, Environment, Analysis*, 6: 325–339.

Guagliardi I, Buttafuoco G, Apollaro C, Bloise A, De Rosa R and Cicchella D 2013. Using gamma-ray Spectrometry and Geostatistics for Assessing Geochemical Behaviour of Radioactive Elements in the Lese Catchment (southern Italy). *Int. J. Environ. Res., 7(3)*:645–658

Hareyama M, Tsuchiya N, Takebe M and Chida T 2000. Two-dimensional measurement of natural radioactivity of granitic rocks by photostimulated luminescence technique. *Geochemical Journal*, 34: 1–9.

Hasterok D and Chapman DS 2011. Heat Production and Geotherms for the Continental Lithosphere, *Earth and Planetary Science Letters*, 307: 59–70.

Holmberg H, Naess E and Evensen JE 2012. Thermal modeling in the Oslo rift Norway. Proceedings of the 37th Workshop on Geothermal Reservoir Engineering Stanford University, Stanford California January 30 – February 1, 2012.

International Atomic Energy Agency (IAEA), 1996. Radiation Safety. Regulation for the safe transport of radioactive material. IAEA Division of Public Information, IAEA-00725 IAEA/PI/A47E.

IAEA, 2003. Guidelines for radioelement mapping using gamma ray spectrometry data. (IAEA-TECDOC-1363, Vienna: International Atomic Energy Agency.

IAEA, 2005. Naturally occurring radioactive materials (iv). Proceeding of an International Conference held in Szezyrk, IAEA TEC DOC-1472, Poland.

Jaupart C, Sclater JG and Simmons G 1981. Heat flow studies: constraints on the distribution of uranium, thorium and potassium in the continental crust. *Earth Planet. Sci. Lett*. 52: 328–344.

Jaupart C and Mareschal JC 2004. Constraints on crustal heat production from heat flow data. In: Rudnick, R. L. (ed) Treatise on Geochemistry Vol. 3: The Crust. Elsevier Science Publishers, Amsterdam, 65–84.

Johnson SS 1979. Radioactivity surveys: Virginia Division of Mineral Resources. *Virginia Miner* 25(2): 9–15

Joshi G, Agarwal KK, Agarwal A, Vidal-Solano JR 2019. Uranium enrichment at North Almora Thrust Zone, Kumaun Lesser Himalaya, Uttarakhand, India. *J. Earth Syst. Sci* 128:211–218

Lima A, Albanese S and Cicchella D 2005. Geochemical baselines for the radioelements K, U and Th in the Campania region, Italy: a comparison of stream-sediment geochemistry and gamma-ray surveys. *Applied Geochemistry*, 20: 611–625.

Malczewski D, Sitarek A, Zaba J and Dorda J 2005. Natural radioactivity of selected crystalline rocks of Iera block. *Prze. Geol*. 53 (3): 237–244

Maxwell O, Wagiran H, Ibrahim N, Kuan Lee S and Sabri S 2013. Comparison of activity concentration of ^{238}U, ^{232}Th and ^{40}K in different layers of subsurface structures in Dei-Dei and Kubwa, Abuja, Northcentral Nigeria. *Radiation Physics and Chemistry*, 91: 70–80

Mukherjee PK, Purohit KK, Saini NK, Khanna PP, Rathi MS and Grosz AE 2007. A stream sediment geochemical survey of the Ganga river headwaters in the Garhwal Himalaya. *Geochem. J*. 41:83–95

Odigi MI, Ezepue MC and Onyeagocha AC 1993. Geochemical evolution of Pan African magmatic rocks

of the basement complex, southwestern Nigeria. *J. African Earth Science*, 17(4): 541–552.

Ojala VJ, Turunen P, Eilu P, Julkunen A and Gehör S 2007. The use of gamma spectrometry in mapping alteration zones in Olkiluoto. Working Report 2007-64, Posiva OY Finland

Olade MA 1978. General features of Precambrian iron ore deposit and its environment at Itakpe ridge, Okene Nigeria. *Trans. Instn. Min. & Metal. Sec. B*, 86: B1–B9

Olade MA and Elueze AA 1979. Petrochemistry of the Ilesha amphibolites and Precambrian crustal evolution in the Pan African domain of SW Nigeria. *Precamb. Res.*, 8: 303–318

Oversby VM 1976. Isotopic ages and geochemistry of Archean and igneous rocks from the Pilbara, Western Australia. *Geochim. Cosmochim. Acta* 40: 817–829.

Plewa M and Plewa S 1992. Petrofizyka, Wydamnictwa Geologiczne, Warszawa, 248–271.

Rybach L 1988. Determination of heat production rate. *In* Hänel, R., Rybach, L. and Stegena, L. (eds.) Handbook of Terrestrial Heat-Flow Determination, Kluwer Academic Publishers, Dordrecht, 125–142.

Sandiford M and McLaren S 2006. Thermo-mechanical Controls on Heat Production Distributions and the Long-term Evolution of the Continents. *In*: Brown, M. and Rushmer, T. (eds.) Evolution and Differentiation of the Continental Crust, *Cambridge University Press*, Cambridge, 67–92.

Sclater JG, Jaupart C and Galson D 1980. The heat flow through oceanic and continental crust and the heat loss from the Earth. *Rev. Geophys*. 18: 269–311.

Shives RBK, Charbonneau BW and Ford KL 1997. The detection of potassic alteration by gamma ray spectrometry- recognition of alteration related to mineralisation. In: Geophysics and Geochemistry at the Millenium, Proceedings of the 4th Decennial International Conference on Mineral Exploration, September 1997, Ontario, Canada, 1100pp.

Slagstad T 2008. Radiogenic heat production of Archean to Permian geological provinces in Norway. *Norwegian Journal of Geology* 88: 149–166.

Taylor SR and McLennan SM 1995. The geochemical evolution of the continental crust. *Rev. Geophys*. 33: 241–265.

Tettey-Larbi L, Darko EO, Schandorf C, Appiah AA, Sam F, Faanu A, Okoh DK, Lawluvi H, Ahyeman BK, Kansaana C, Amoah PA, Osei RK, Agalga R and Osei S 2013. Gross alpha and beta activity and annual committed effective dose due to natural radionuclides in some medicinal plants community used in Ghana. *Int. J. Sci. Technol*. 3 (4): 217–229

Trindade MJ, Prudêncio CI, Burbidge CI, Dias MI, Cavdoso G, Marques R and Rocha F 2013. Distribution of naturally occurring radionuclides (K, Th, and U) in weathered rocks of various lithological types from the Uranium bearing region of Fornos De Algodres Portugal. *Mediterranean Archeology and Archaeometry*, 13(3):71–79.

UNSCEAR 2000. Sources and effects of ionising radiation. United Nations Scientific Committee on the Effects of Atomic Radiation Report to the General Assembly, with scientific annexes, I

Verdoya M, Chiozzi P and Pasquale V 2001. Heat-producing radionuclides in metamorphic rocks of the Brianconnais–Piedmont Zone (Maritime Alps). *Eclogae Geol Helv* 94:1–7

Waples DW 2001. A new model for heat flow in extensional basins: radiogenic heat, asthenospheric heat, and the McKenzie model. *Natural Resources research*, 10, 3

Wasserburg GJ, MacDonald GJF, Hoyle F and Flower WA 1964. Relative contributions of uranium, thorium and potassium to heat production in the Earth. *Science* 143: 465–467

Willmot NM, Daly JS and the IRETHERM team 2015. The Contribution of Radiogenic Heat Production Studies to Hot Dry Rock Geothermal Resource Exploration in Ireland. Proceedings of World Geothermal Congress Melbourne, Australia, 19-25 April 2015, 1–11

Xinwei L, Lingqing W and Xiaodan J 2006. Radiometric analysis of Chinese commercial granites. *Journal of Radioanalytical and Nuclear Chemistry* 267(3): 669–673